ICAS-88-4.2.2

NUMERICAL SIMULATION OF AN UNSTEADY TURBULENT FLOW PAST A SUDDEN EXPANSION

Yves Gagnon [1] and André Giovannini [2]

[1] Assistant Professor
Centre universitaire St-Louis Maillet
Université de Moncton
Edmundston, N.B., Canada

[2] Research Scientist
ONERA / CERT
B.P. 4025
Toulouse, France

Abstract

This work presents the results of numerical simulations of an unsteady turbulent flow in a two-dimensional channel that incorporates a sudden expansion in the form of two backward-facing steps. The Random Vortex Method, a direct simulation method, is used in this study. This grid-free, Lagrangian method solves the unaverage Navier-Stokes equations and the continuity equation, with the appropriate boundary conditions, using a formulation in vorticity variables. An extensive set of numerical results is presented and compared with experimental results published in the literature. The unsymmetric behaviour of the flow, as observed experimentally, is simulated accurately using the Random Vortex Method.

I. Introduction

This paper presents the results of numerical simulations of an unsteady turbulent flow in a two-dimensional channel that incorporates a sudden expansion in the form of two backward-facing steps, Figure 1. The choice of this fondamental geometry is based on the availability in the literature, of extensive experimental results concerning velocity profiles and pressure fields. Moreover, the practical interests of this geometry is evident, in particular, such computational simulations are necessary to understand the flow instabilities and the principal frequencies governing physical applications. Those basic studies are essential in the understanding of physical phenomenas such as induced vibrations, heat and mass transfers and unsteady combustion waves generated by the flow instabilities.

The flow in this geometry has been extensively studied experimentally in the laminar and turbulent regimes by Mehta (1), Abbot and Kline (2), Durst et al. (3), Restivo and Whitelaw (4) and Smyth (5) for geometries having expansion ratios of 2 and 3. What is remarkable with those studies is the important and permanent unsymmetry in one or the other recirculation zone for fluids having Reynolds numbers above a few tens. With all the imaginable experimental precautions taken, these authors could not put into evidence any geometric defaults in the experimental apparatus that could explain this behaviour of the flow. Once that the flow was attached on one wall, thus making a longer recirculation zone on the other wall, the flow stays attached to that wall until a perturbation would make it flip to the other wall. The same phenomena is observed in fluidics and applied, for example, in industrial logical circuits ("or" cells).

The objectives of modern numerical analysis are the prediction of turbulent statistics and the topology of all the vortical structures present in the flow field. Classical methods, Durst et al. (3), Acrivos et al.(6), deal with the average Navier-Stokes equations. The solution is performed on a grid and the resolution is obtained by closure modeling or by an integral approach. The main drawbacks of these methods are the non-universality of the modeling constants, the numerical diffusion introduced by the Eulerian grid and the inability to solve unsteady and multi-scale flows such as for the geometry described above. Naturally, the recirculation zones obtained by classical methods are symmetric.

In order to overcome these difficulties, direct simulation methods have been developed. The Random Vortex Method RVM, Chorin (7), used for this study falls in that category. This grid-free, Lagrangian method solves the unaverage Navier-Stokes equations and the continuity equation, with the appropriate boundary conditions, using a formulation

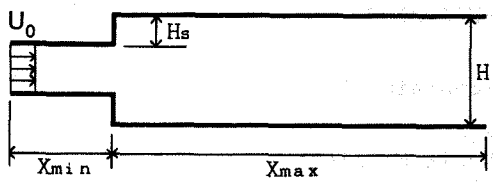

Figure 1. The geometry investigated.

in vorticity variables. The satisfaction of the no-slip condition on solid walls allows for the generation of an appropriate amount of circulation in the form of discrete vortex elements. The advancement of the computation is performed by moving this vorticity field according to the vorticity transport equation which is solved in two fractional steps: convection and diffusion. The velocity field is recovered from the vorticity field by integrating the continuity equation and the vorticity definition. Finally, the instantaneous pressure fields are obtained by solving a Poisson equation that relates the pressure to the velocity field. Applications of the RVM have been presented by Ghoniem and Sethian (8), Ghoniem and Gagnon (9) and Giovannini and Karagiannis (10). In the first case, qualitative results with no comparison to experimental results are presented for a single-step recirculating flow for laminar and turbulent regimes. In the second case, a careful numerical study is performed on a single-step recirculating flow in the laminar regime. The comparison of the numerical and experimental results are in very good agreement. In the third case, the study of the fluid flow inside a combustion engine is presented. An extension of the method is made to solve for compressible flows.

The objective of this work is to show the accuracy and the convergence of the Random Vortex Method to solve the fluid flow equations in the turbulent regime. To reach this objective, different numerical results in the form of velocity profiles, pressure profiles, vorticity fields, streamlines and turbulent statistics are presented and compared to experimental data when available.

In section II, the formulation and a brief description of the numerical scheme are presented. In section III, results are presented for an unsteady turbulent flow in a two-dimensional channel that incorporates a sudden expansion in the form of two backward-facing steps. The different instantaneous fields and the corresponding average fields are presented and compared to experimental results. A brief discussion and the possible extensions of this work presented in section IV conclude this paper.

II. Numerical Scheme

Incompressible flows are governed by the continuity equation, Eq. 1, and the Navier-Stokes equations, Eqs. 2 . In a normalized form,

$$\nabla \cdot \mathbf{u} = 0 \qquad (1)$$

and

$$\frac{\partial \mathbf{u}}{\partial t} + \mathbf{u} \cdot \nabla \mathbf{u} = -\nabla p + \frac{1}{R}\nabla^2 \mathbf{u} \qquad (2)$$

where $\mathbf{u} = (u,v)$ is the velocity vector, p is pressure and t is time. The Reynolds number R is defined as $\rho U H/\mu$, where ρ is the density, μ is the viscosity, U is a reference velocity and H is a length reference. The geometry investigated is a two-dimensional channel that incorporates a large sudden expansion of ratio 2 in the form of two backward-facing steps, Figure 1. The boundary conditions are the no-slip and the no-normal velocities on solid walls and an imposed inlet velocity profile. Therefore,

$\mathbf{u} = (0,0)$ on walls

$\mathbf{u} = (U_0,0)$ at the inlet section

The outlet boundary condition is explained in section II.2 .

All the physics of the fluid flow is contained within the above formulation. Because of the impossibility to obtain an analytical solution to the problem, a numerical scheme is devised. The scheme used in this study is the Random Vortex Method (7) as presented in the next section.

II.1 Random Vortex Method

In order to overcome the non-linearity of the Navier-Stokes equations, the RVM uses a hybrid algorithm to solve for the velocity field and the pressure field. The velocity field is obtained using a formulation in vorticity variables (u,v,ω) instead of using a formulation in primitive variables (u,v,p). The pressure field is obtained by solving a classical Poisson equation that relates the pressure to the space derivative of the velocity, as presented in section II.3 .

The algorithm to solve for the velocity field starts by defining the vorticity variable $\vec{\omega}$,

$$\vec{\omega} = \nabla \times \mathbf{u} \qquad (3)$$

In two dimensions, the vorticity $\vec{\omega}$ is a scalar ω ,

$$\vec{\omega} = (0,0,\omega) = \left(0\ ;\ 0\ ;\ \frac{\partial v}{\partial x} - \frac{\partial u}{\partial y}\right)$$

By taking the curl of the Navier-Stokes equations and using the fact that the divergence of the velocity vector is zero,

Eq. 1, we obtain the vorticity transport equation,

$$\frac{\partial \omega}{\partial t} + \mathbf{u} \cdot \nabla \omega = \frac{1}{R} \nabla^2 \omega \qquad (4)$$

In this method, we use Eq. 4 to transport the vorticity field over a time step Δt. We then use Eq. 3 and Eq. 1 to obtain the corresponding velocity field. Eq. 4 is solved in two fractional steps, convection and diffusion, Eq.5 and Eq. 6, respectively;

$$\frac{\partial \omega}{\partial t} + \mathbf{u} \cdot \nabla \omega = 0 \qquad (5)$$

$$\frac{\partial \omega}{\partial t} = \frac{1}{R} \nabla^2 \omega \qquad (6)$$

The convection step, Eq. 5, of the vorticity transport equation is solved by performing Lagrangian displacements of a set of discrete vortex elements that discretize the vorticity field, $\omega(x,y)$. The solution of Eq. 5 is developed using the definition of a streamfunction Ψ and by using Green's function. The solution is given by the Biot-Savart Law,

$$\mathbf{u}(x,y) = \int \mathbf{k}(x - x', y - y')\, \omega(x', y')\, dA' \qquad (7)$$

with $$\mathbf{k}(x,y) = -\frac{1}{2\pi} \frac{(y, -x)}{r^2}$$

$\mathbf{k}$ is the integral kernel of the Poisson equation with $r^2 = x^2 + y^2$. The vorticity field in our domain of computation is dicretized among small elements to form particles of vorticity, or vortex blobs, which carry an invariant and finite amount of δA_i circulation. Each element that discretizes the vorticity field over an area has an amount of circulation that satisfies the definition of the circulation

$$\Gamma_i = \int_{\delta A_i} \omega \, dA$$

$$\Gamma_i \cong \omega(x, y)\, dA_i \qquad (8)$$

To eliminate the singularity caused by a point vortex, the vorticity carried by each element is distributed according to a core function with a finite radius δ, Chorin and Bernard (11), Kuwahara and Takami (12). The core function f(r) which can take several forms (8,13,14,15,16) plays a similar role as interpolating polynomials in finite-difference schemes and base functions in finite-element formulation. The resulting approximation of the vorticity distribution is

$$\omega(x, y) = \sum_{i=1}^{n} \Gamma_i f_\delta(x, y) \qquad (9)$$

The velocity produced by a distribution of discrete vortex blobs with finite and invariant cores is obtained by substituting Eq. 9 into Eq. 8;

$$\mathbf{u}_\delta(x, y) = \sum_{i=1}^{n} \Gamma_i \mathbf{k}_\delta(x - x', y - y') \qquad (10)$$

where $$\mathbf{k}(x,y) = -\frac{1}{2\pi} \frac{(y, -x)}{r^2} \kappa\left(\frac{r}{\delta}\right) \qquad (11)$$

and $$\kappa(r) = 2\pi \int_0^r r\, f(r)\, dr \qquad (12)$$

The choice of the core function in this study is the same as the one chosen by Ghoniem and Gagnon (9),

$$f(r) = \frac{1}{2\pi r} \quad \text{for} \quad r \le 1$$
$$f(r) = 0 \quad \text{for} \quad r > 1 \qquad (13)$$

In Lagrangian form, the convection equation takes the form of a simple differential equation,

$$\frac{d\chi}{dt} = \mathbf{u}(\chi(x, y, t)) \qquad (14)$$

where $\chi(x,y,t)$ is the trajectory of a particle that starts at $\chi(x,y,0) = X$. In a discrete form, Eq. 14, representing the motion of vortex blobs, takes the following form

$$\frac{d\chi_j}{dt} = \sum_{i=1}^{n} \sum_{j \neq i} \Gamma_i \mathbf{k}_f(\chi_i - \chi_j) \qquad j = 1,2, \ldots n \qquad (15)$$

The vortex elements that discretize the vorticity field are created and up-dated to satisfy the no-slip condition on solid walls. This is done with the vortex sheet algorithm, Chorin (17) and Ghoniem and Gagnon (9).

The second step of the vorticity transport equation, diffusion, Eq. 6, is solved by implementing random walk movements to the vortex blobs according to Gaussian statistics. Effectively, the solution of the one-dimensional form of Eq. 6, given by the Green function

$$Gr(y,t) = \sqrt{\frac{R}{4\pi t}} \exp\left(\frac{-R}{4t} y^2\right) \qquad (16)$$

is identical to the probability density function of a Gaussian random variable with a zero mean and a standard deviation σ,

$$P(\eta,t) = \sqrt{\frac{1}{2\pi r^2}} \exp\left(\frac{-1}{2r^2} \eta^2\right) \qquad (17)$$

if $\sigma = \sqrt{2t/R}$. In two dimensions, the Green function of Eq. 6 is given by:

$$Gr'(x,y,t) = \frac{R}{4\pi t} \exp\left(\frac{-R}{4t} \left(x^2+y^2\right)\right) \qquad (18)$$

which is equivalent to

$$Gr'(x,y,t) = Gr(x,t)\, Gr(y,t) \qquad (19)$$

Accordingly, the corresponding probability density function is given by

$$P'(\eta_x,\eta_y,t) = P_1(\eta_x,t)\,P_2(\eta_y,t) \qquad (20)$$

Therefore, the solution of the diffusion step of the vorticity transport equation is performed by imposing stochastic displacements of the vortex elements in two perpendicular directions. Each displacement is generated randomly from two sets of independant Gaussian random numbers, with each set having a zero mean and a standard deviation $\sigma = \sqrt{2\Delta t/R}$. Performing random walks at each time step and adding the displacements to obtain the total displacement at time t is possible because of the linearity of the diffusion equation.

The Random Walk Algorithm is compatible with discrete vortex schemes because of its Lagrangian grid-free form. The total transport of vortex elements over a time step is obtained by adding the two fractional steps of the vorticity transport equation, convection and diffusion:

$$\chi_j(x_j,y_j,t+\Delta t) = \chi_j(x_j,y_j,t) + \mathbf{u}(x_j,y_j,t)\,\Delta t + (\eta_x,\eta_y) \qquad (21)$$

In this equation $\mathbf{u} = \mathbf{u}_\delta + \mathbf{u}_p$, where $\mathbf{u}$ is the total velocity field due to the vortex elements ($\mathbf{u}_\delta$, Eq.10) and the potential flow ($\mathbf{u}_p$) that satisfies the potential boundary condition.

The potential flow is solved using conformal mapping and using the image system of the vortex elements. This allows for a grid-free solution and for relatively high accuracy along the boundaries and at points of separation. For the geometry considered in this study, Figure 1, the transformation function is derived using the Schwarz-Christoffel theorem, which gives the following transformation:

$$F(\zeta) = \frac{d\zeta}{dz} = \pi\zeta\sqrt{\frac{\zeta^2-2^2}{\zeta^2-1}} \qquad (22)$$

The inverse transformation, $z = z(\zeta)$ is obtained by integrating Eq. 22,

$$z = \frac{1}{2\pi}\left(\ln\frac{1+t}{1-t} - \frac{1}{2}\ln\frac{2+t}{2-t}\right) \qquad (23)$$

$$t = \sqrt{\frac{2^2-\zeta^2}{1-\zeta^2}}$$

II.2 Algorithm

The algorithm is presented schematically in the form of a block diagram on Figure 2. The actual computation starts with a potential flow within the domain. Vorticity is generated along solid walls to cancel the slip velocity. That vorticity is then convected and diffused, thus creating a new vorticity field and a corresponding rotational velocity field, Eq. 10. A new total velocity field is computed and new vortex elements are generated along solid walls. The new vorticity field is then convected, Eq. 15, and diffused, thus updating this new vorticity field, Eq. 21. The loop starts again by computing a new total velocity field and by updating the vorticity field. The flow develops and a solution is performed until the averaging of physical quantities, such as velocity profiles, become independant of the amount of time steps necessary to make the average.

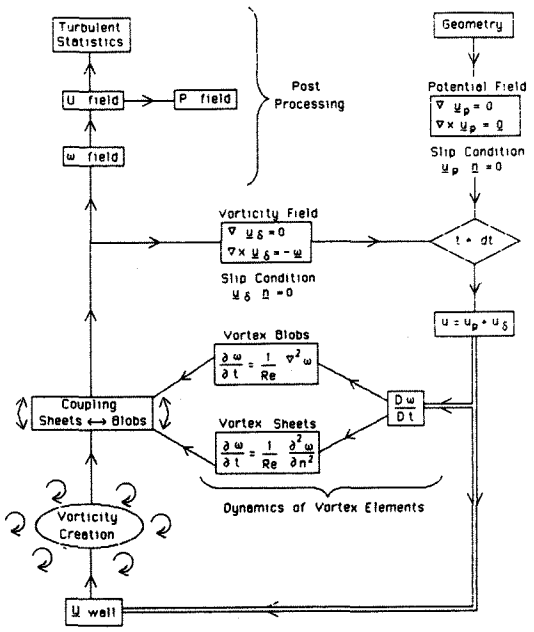

Figure 2. Block diagram of the Random Vortex Method.

The exit boundary condition needs to be analysed. Since vortex elements are being generated at every time step, the number of vortex blobs can become excessively large. The exit boundary condition makes that the number of elements reaches a maximum and becomes relatively stable. What is done is that the blobs that reach a position longer than the computational domain are deleted, there effect on the dynamics of the flow being negligibly small. The length of the computational domain is chosen to be long enough so that the effect of the exit boundary condition does not modify the dynamics of the flow in the regions of interest, namely the recirculation zones, the reattachment and the redevelopment of the flow inside the channel.

A comprehensive analysis of the effect of the length of the channel and the other numerical parameters can be found in Ghoniem and Gagnon (9).

II.3 Pressure

The Random Vortex Method solves the fluid equations using the vorticity variables, u, v and ω. The solution obtained gives the velocity field as a function of position and time. No information about the pressure field is obtained. However, the pressure can be recovered by solving a Poisson equation that relates the pressure field to the velocity field, as presented below.

Fluid flows are governed by the continuity and the Navier-Stokes equations, Eqs. 1 and 2. By taking the divergence of Eq. 2 and by using Eq.1, we get the following Poisson equation

$$\nabla^2 p = 2\left(\frac{\partial u}{\partial x}\frac{\partial v}{\partial y} - \frac{\partial u}{\partial y}\frac{\partial v}{\partial x} \right) \qquad (24)$$

where ∇^2 is the Laplacian operator. The solution of this equation is obtained using a finite- difference scheme on a grid inside the channel (18). The boundary conditions on solid walls and the outlet section are of the Neumann type. These boundary conditions are obtained from the full Navier-Stokes equations, i.e. the time- dependant equations. A Dirichlet condition is imposed at the inlet section. We then compute the velocity field at every time step on the grid, from which the instantaneous pressure field is calculated. Average pressure fields are then deduced.

The next section presents the solutions obtained using the Random Vortex Method. Comparisons are made with experimental results to show the accuracy and the convergence of the method.

III. Solution

The geometry investigated is a channel that incorporates a sudden expansion in the form of two backward-facing steps, Figure 1. The type of flow studied is in the unsteady turbulent regime. The flow starts as a uniform flow at $X_{min} = -1.0H$, H being the height of the channel downstream of the step. The flow develops in the inlet section forming two boundary layers. At the step, the flow separates from the horizontal walls, thus forming two shear layers and two recirculation zones at both corners. Further downstream, the two shear layers diffuse and the flow redevelops after the recirculation zones. Even though the geometry is relatively simple, the flow within is very complicated because of the dynamics of the flow structures. The interactions between the shear layers and the recirculation zones formed of large eddies make the flow to have an unsteady behaviour characterized by the formation, the pairing and the diffusion of those large eddies.

Experimental results for this type of flow show that the recirculation zones are unsymmetric in size and length, (1, 2, 3, 4, 5). The unsymmetry is found on one or the other zone and is permanent until a perturbation would modify the flow and make it flip to the other wall. The experimental results chosen to compare our numerical computations are those by Mehta (1). The experiment was performed with a turbulent flow with a Reynolds number of 10^5 based on a uniform axial velocity in the inlet channel and on the hydraulic radius of the inlet channel. The experimental results correspond to a two-dimensional flow, hence our two-dimensional model, if correct, should predict the behaviour of this flow. The following numerical results along with comparisons with the corresponding experimental results show the accuracy of the Random Vortex Method to predict the behaviour of complicated, unsteady recirculating flow in the turbulent regime.

The solution is initiated with a potential flow inside the channel. Vorticity in the form of vortex sheets are then generated along solid walls to annihilate the slip velocity. These vortex sheets are then diffused and convected outside of the sheet layer to become vortex blobs. At every subsequent time steps, a number of vortex sheets is generated along solid walls and another number is transferred into vortex blobs. The transformation of blobs to sheet is also possible, but less frequent. The number of vortex blobs N as a function of the number of time step with $\Delta t = 0.05$ is shown on Figure 3. After 200 time steps,

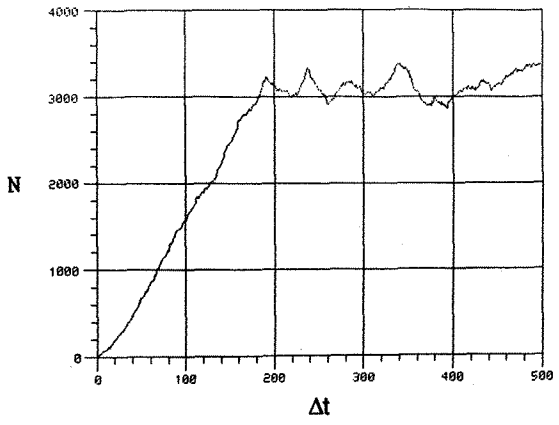

Figure 3. Number of vortex blob N as a function of the number of time step t.

the flow reaches a stationary state. Averaging of physical quantities is then possible starting from this time step. The numerical parameters were chosen to have an optimum solution and to eliminate the numerical diffusion, as presented by Ghoniem and Gagnon (9).

We first present instantaneous fields to show the unsteady nature of the flow. Figure 4 presents instantaneous velocity profiles at different sections represented by the dashed lines. The dotted lines represent the experimental average velocities of Mehta and the solid lines represent our numerical velocities. The first channel shows the streamwise velocity profiles and the second channel shows the cross-stream velocity profiles (no experimental comparisons). The instantaneous velocity profiles are more rugged than average velocity profiles and the cross-stream velocities are smaller than the streamwise velocities. The corresponding vorticity field for this flow is presented on Figure 5. Each vortex blob is indicated by a small point and the line attached depicts its instantaneous velocity vector. We can see, from this figure, the different eddy structures that form the recirculation zones. The recirculation zone on the top part of the channel is formed of two large eddies and the bottom recirculation zone is formed of one smaller eddy. Figure 6 shows the corresponding instantaneous

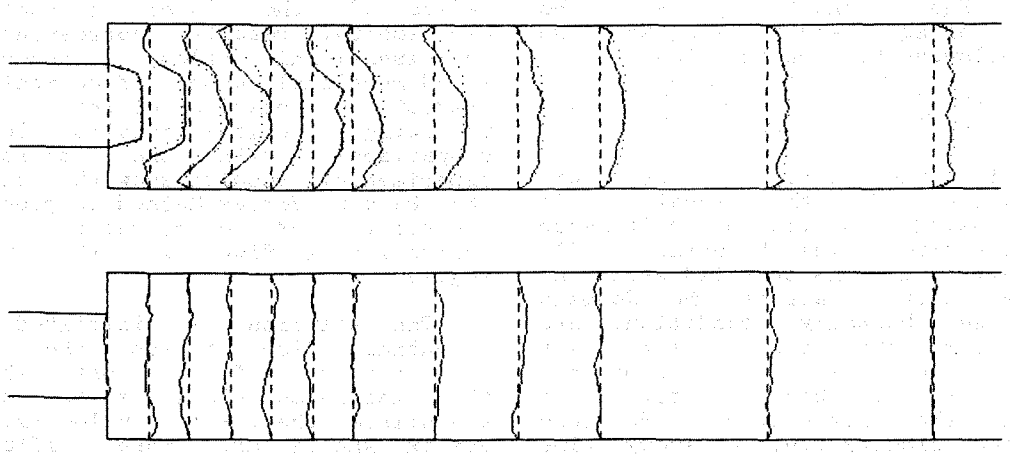

Figure 4. Instantaneous velocity profiles. The first channel shows the streamwise velocity profiles and the second channel shows the cross-stream velocity profiles. The dotted and the solid lines are the experimental and the numerical velocities, respectively.

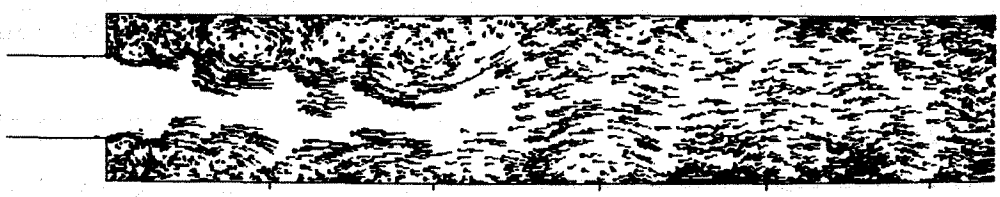

Figure 5. Corresponding vorticity field for the flow of Figure 4.

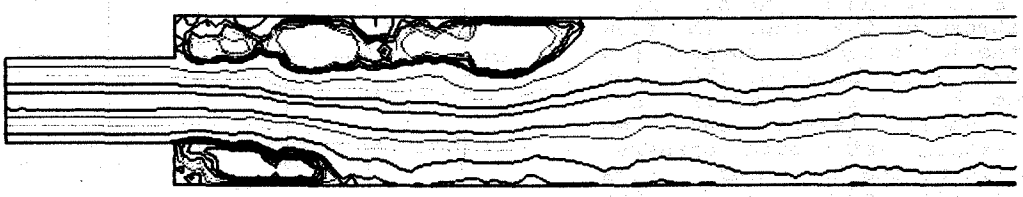

Figure 6. Corresponding streamline plot for the flow of Figures 4 and 5.

streamline plot for the flow presented on Figures 4 and 5. We can clearly see the different structures forming the two recirculation zones. The unsteady and unsymmetric nature of the flow is clearly indicated on the last three figures.

Of more important aspect for the assessment of our numerical model is the comparison of corresponding experimental and numerical results. Average velocity profiles for different sections are presented on Figure 7. The first channel compares the average streamwise velocity profiles. The dotted lines are the experimental results and the solid lines are the numerical results at the same sections, indicated by the dashed lines. We can appreciate the global accuracy between the experimental and numerical results. Interesting features can be pointed out by looking closer at those results. The experimental and numerical profiles at the step are practically the same. We can also see that the numerical model predicts an unsymmetric flow field as obtained experimentally. The size and the length of the two recirculation zones are different from each other. Further downstream, the flow redevelops and tends toward a fully developed flow at about 4 - 5 channel heigths downstream of the step. The second channel presents the average cross-stream velocity profiles. We can see that on the average, the cross-stream velocities are very small in comparison to the streamwise velocities. The corresponding average streamline plot is presented on Figure 8. We can see the different length and size of the two recirculation zones.

Turbulent kinetic energy u'^2, v'^2 and shear stress $u'v'$ obtained numerically, are presented on Figure 9 and compared to experimental data. On the three channels, the dashed, dotted and solid lines represent the reference section, the experimental and the numerical results, respectively. The

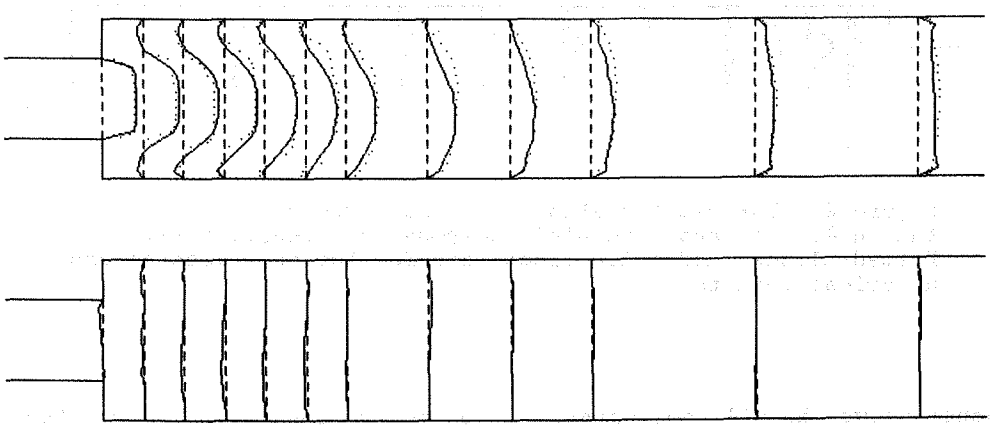

Figure 7. Average velocity profiles. The first channel shows the streamwise velocity profiles and the second channel shows the cross-stream velocity profiles. The dotted and solid lines are the experimental and the numerical velocities, respectively, at different sections represented by the dashed lines.

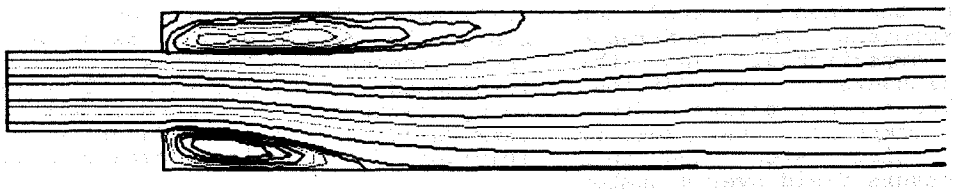

Figure 8. Corresponding streamline plot for the flow presented on Figure 7.

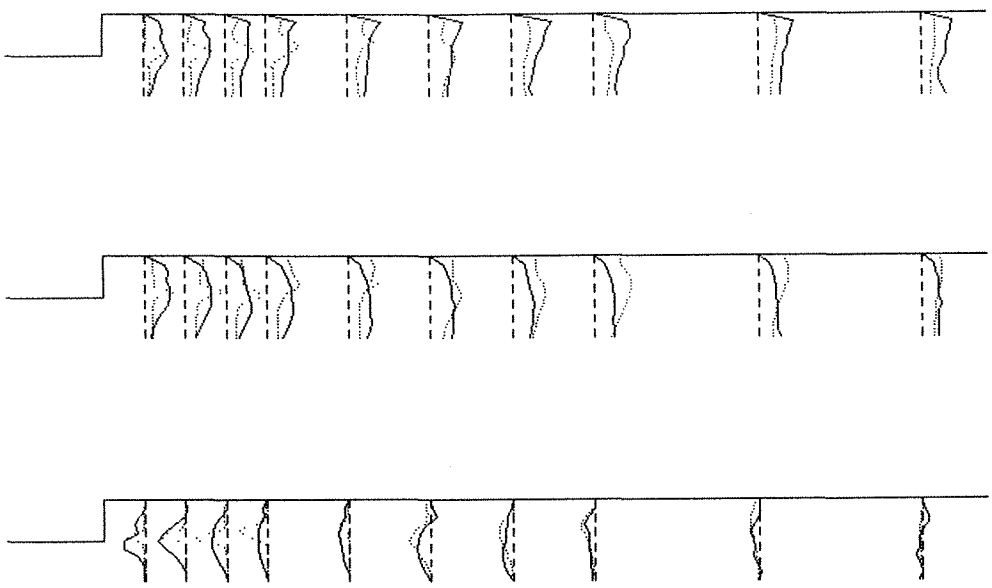

Figure 9. Turbulent statistics. The three channels are for the u'^2, v'^2 and the $u'v'$ components, respectively. Dotted lines and solid lines are for the experimental and numerical results.

first channel shows the u'^2 component; the second channel, the v'^2 component and the third channel, the $u'v'$ component. We note that, globally, the level of values of u'^2 and v'^2 (15%), and $u'v'$ (5%) are correct, but the results obtained from a sample of 200 time steps are not stationnary and are still evolving.

The pressure field can be recovered from the velocity field, as presented in section II.3 . The average pressure field over 200 time steps is presented on Figure 10. Once again, the dashed, dotted and solid lines represent the reference section, the experimental and the numerical pressure coefficient respectively. The average pressure field is obtained by computing the pressure field at every time step and then averaging the pressure field over a number of time steps. The solution using this method is exact compared to the method of computing the pressure field from the average velocity field. The last method is incorrect because of the non-linearity in the source term of the Poisson equation, and the presence of the unsteady term coming from the Navier-Stokes equations, which give the downstream boundary condition for the pressure equation, Eq. 24 . The comparison of numerical and experimental results show that the initial and final pressure in the channel are in good comparison, thus indicating the accuracy in solving the adverse pressure gradient. However, in the region of strong velocity dynamics, the numerical pressure solution does not compare with the experimental pressure. This is most probably due to the pointwise instantaneous error in the velocities because of the use of a core function to distribute the vorticity over an area. Since the pressure is based on those instantaneous velocities, error is introduced on the pressure. Studies are being performed to assess the errors introduced by the core functions on the solution of the Navier-Stokes equations.

Figure 11 shows the average pressure at every point in the channel. This is shown in the form of a three-dimensional curve where the heigth of the curve indicates a relative value of the pressure coefficient. Instantaneous pressure curves are more rugged and are dependant on the large eddy structures inside the channel, (18).

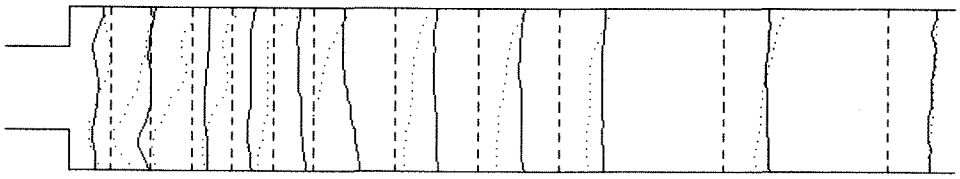

Figure 10. Comparison of the average pressure coefficient profiles for the flow corresponding to Figure 7. Dotted lines and solid lines are for the experimental and numerical results.

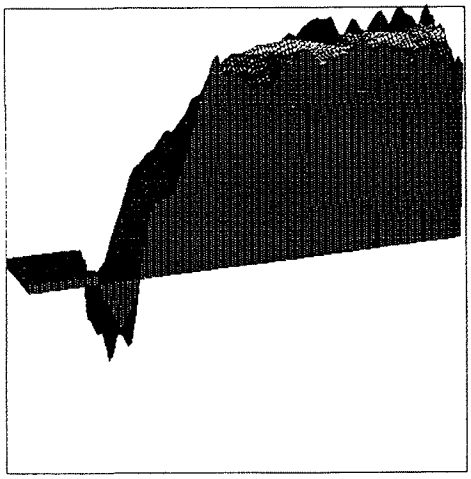

Figure 11. Three-dimensional pressure surface for the flow presented on Figure 7.

IV. Conclusion

The results presented in this paper show the accuracy of the Random Vortex Method to simulate time-dependant flows at high Reynolds numbers. Comparisons of numerical and experimental velocity profiles have shown the ability of the method to predict the velocities at any point inside the channel. Because of the unsteadiness of the simulations, insights on the dynamics and the structures of a flow past a sudden expansion are shown. We have seen limitations of the method to accurately predict the turbulent statistics and the instantaneous pressure fields. However, we have mentionned that the average pressure field computed from the average velocity field is inaccurate and gives a solution largely different than using instantaneous velocity fields and then averaging the pressure field.

Studies are being performed to study the influence on the accuracy of using core functions to distribute the vorticity field into vortex blobs. Possible extensions of this work being developed include the simulation of pulsed flow, particle tracking, multi-phase flow and flame-front propagation.

Acknowledgment

The support for this work is from the French Ministry of Defence (Direction des recherches et études techniques, France) for (2); and, the Ministère de l'extérieur, France, and by the Centre universitaire St-Louis Maillet of the Université de Moncton for (1).

References

1) Metha P.R., 1981. "Separated Flow Through Large Sudden Expansions", J. Hydr. Div., Vol 107, No HY4, pp. 451-460.

2) Abbot D.C. and Kline S.J., 1961. "Experimental Investigations of Subsonic Turbulent Flow over Single and Double Backward-facing Steps", J. Basic Engrn., Vol D84, pp. 317-325.

3) Durst F., Melling A. and Whitelaw J.H., 1974. "Low Reynolds Number Flow over a Plane Symmetric Expansion", J. Fluid Mech., Vol 64, pp. 111-128.

4) Restivo A. and Whitelaw J.H., 1978. "Turbulence Characteristics of the Flow Downstream of a Symmetric Plane Sudden Expansion", ASME, Non-steady Fluid Dynamics, San Fransico, USA.

5) Smyth F., 1976. "Experimental Study of Turbulence in Plane Separated Flows", Proc. ISL/AGARD Workshop on laser anemometry, p. 233.

6) Acrivos A. and Shrader M.L., 1982. "Steady Flow in a Sudden Expansion at High Reynolds Numbers", Physics of Fluids, Vol 25 (6).

7) Chorin A.J., 1973. "Numerical Study of Slightly Viscous Flow", J. Fluid Mech., Vol 57, pp. 785-796.

8) Ghoniem A.F. and Sethian J.A., 1985. "Dynamics of Turbulent Structure in Recirculating Flow: A Computational Study", 23rd Aerospace Sciences Meeting, Reno, Nevada, AIAA-85-0146.

9) Ghoniem A.F. and Gagnon Y., 1987. "Numerical Investigation of Recirculating Flow at Moderate Reynolds Numbers", J. Compt. Phys., Vol 68, No 2, pp. 346-377.

10) Giovannini A. and Karagiannis F., 1987. "A New Predicting Tool for the Flow Field inside the Cylinder of an Internal Combustion Engine", ICIAM, Paris, France.

11) Chorin A.J. and Bernard P., 1973. "Discretization of a Vortex Sheet with an Example of Roll-up", J. Compt. Phys., Vol 13, pp. 423-428.

12) Kuwahara K. and Takami H., 1973. "Numerical Studies of Two-dimensional Vortex Motion by a System of Point Vortex", J. Phys. Soc. Japan, Vol 34, pp. 247-252.

13) McCracken M.F. and Paskin C.S., 1980. "Vortex Methods for Blood Flow through Hearth Valves", J. Compt. Phys., Vol 35, pp. 183-205.

14) Ghoniem A.F., Chorin A.J. and Oppenheim A., 1982. "Numerical Modeling of Turbulent Flow in a Combustion Tunnel ", Phil. Trans. R. Soc. London, A 304, pp. 303-325.

15) Cheer A.Y., 1983. Center for Pure and Applied Mathematics, University of California, Berkeley, Report PAM-145.

16) Sethian J.A., 1984. "Turbulent Combustion in Open and Closed Vessels", J. Compt. Phys., Vol 54, pp. 425-456.

17) Chorin A.J., 1978. "Vortex Sheet Approximation of Boundary Layers", J. Compt. Phys., Vol 27, pp. 423-442.

18) Gagnon Y. and Giovannini A., 1988. "Numerical Simulation of a Recirculating Flow at High Reynolds Number", The Physics of Fluids, in preparation